

Received 5 October; accepted 15 October 1998.

1. Simpson, J. J. Evidence of heavy neutrino emission in beta-decay. *Phys. Rev. Lett.* **54**, 1891–1893 (1985).
2. Sur, B. *et al.* Evidence for the emission of a 17-keV neutrino in the  $\beta$  decay of  $^{14}\text{C}$ . *Phys. Rev. Lett.* **66**, 2444–2447 (1991).
3. Datar, V. M., Baba, C. V. K., Bhattacharjee, S. K., Bhuiyana, C. R. & Roy, A. Search for a heavy neutrino in  $\beta$ -decay of  $^{35}\text{S}$ . *Nature* **318**, 547–548 (1985).
4. Stoeffl, W. & Decman, D. J. Anomalous structure in the beta decay of gaseous molecular tritium. *Phys. Rev. Lett.* **75**, 3237–3240 (1995).
5. Belesov, A. I. *et al.* Results of the Troitsk experiment on the search for the electron antineutrino rest mass in tritium beta decay. *Phys. Lett. B* **350**, 263–272 (1995).
6. Koonin, S. E. Environmental fine structure in low-energy  $\beta$ -particle spectra. *Nature* **354**, 468–469 (1991).
7. Ashley, C. A. & Doniach, S. Theory of extended x-ray absorption edge fine structure (EXAFS) in crystalline solids. *Phys. Rev. B* **11**, 1279–1288 (1975).
8. Booth, N., Cabrera, B. & Fiorini, E. Low temperature particle detectors. *Annu. Rev. Nucl. Part. Sci.* **46**, 471–532 (1996).
9. Swift, A. M. *The Study of the  $\beta$  Environmental Fine Structure Applied to the  $\beta$ -decay of  $^{187}\text{Re}$*  1–16 (Preprint INFN/BE-97/02, INFN, Genoa, 1997).
10. Lee, P. A., Citrin, P. H., Eisenberg, P. & Kincaid, B. M. Extended x-ray absorption fine structure—its strengths and limitations as a structural tool. *Rev. Mod. Phys.* **53**, 769–806 (1981).
11. Lee, P. A. & Pendry, J. Theory of the extended x-ray absorption fine structure. *Phys. Rev. B* **11**, 2795–2811 (1975).
12. Eckerlin, P. & Kandler, H. *Landolt Börnstein New Series* 6, 21 (eds Hellwege, K. H. & Hellwege, A. M.) (Springer, Berlin, 1971).
13. Stahle, C. K., Kelley, R. L., McCammon, D., Moseley, S. H. & Szymkowiak, A. E. Microcalorimeter array for high resolution soft x-ray spectroscopy. *Nucl. Instrum. Methods Phys. Res. A* **370**, 173–176 (1996).
14. Galeazzi, M. Status of the rhenium beta experiment for neutrino mass study. *Nucl. Phys. B (Proc. Suppl.)* **66**, 203–206 (1998).
15. Fontanelli, F., Galeazzi, M., Gatti, F., Swift, A. M. & Vitale, S. *Nucl. Instrum. Methods Phys. Res. A* (submitted).
16. Caso, C. *et al.* Review of particle physics. *Eur. Phys. J. C* **3**, 1–784 (1998).

**Acknowledgements.** This work was supported by INFN and the EC-HCM Programme ‘Cryogenic Detectors’.

Correspondence and requests for materials should be addressed to S.V. (e-mail: vitale@ge.infn.it).

## Lateral drag of spin coherence in gallium arsenide

J. M. Kikkawa & D. D. Awschalom

Department of Physics, University of California, Santa Barbara, California 93106, USA

The importance of spin-transport phenomena in condensed-matter physics has increased over the past decade with the advent of metallic giant-magneto-resistive systems and spin-valve transistors<sup>1</sup>. An extension of such phenomena to semiconductors should create possibilities for seamless integration of ‘spin electronics’ with existing solid-state devices, and may someday enable quantum computing schemes using electronic spins as non-local mediators of coherent nuclear spin interactions<sup>2</sup>. But to realize such goals, spin transport must be effected without destroying the relevant spin information. Here we report time-resolved optical studies of non-local Faraday rotation in n-type bulk gallium arsenide, which show macroscopic lateral transport of coherently precessing electronic spins over distances exceeding 100 micrometres. The ability to drag these spin packets by their negative charge, without a substantial increase in spin decoherence, is a consequence of the rather weak entanglement of spin coherence with orbital motion in this system<sup>3</sup>.

In Faraday-rotation measurements of spin precession within semiconductors, excitation by normally incident pulses of circularly polarized light produces a conduction-band spin imbalance in a superposition of spin states whose degeneracy is removed by a transverse (in-plane) magnetic field. The quantum coherent beating between these states results in Larmor precession of the classical spin vector, whose ensemble-average projection along the sample normal is measured by a time-delayed, linearly polarized probe pulse. The decay time of the transverse spin polarization,  $T_2^+$ , measures an upper limit on extra-electronic spin decoherence and conceals only rotationally invariant intra-electronic processes, which preserve the total electron magnetization<sup>4</sup>. The divergence

of  $T_2^+$  with reduced excitation and magnetic field complicates its measurement by traditional scans of the pump–probe delay,  $\Delta t$ , because relative polarization changes over nanosecond intervals are small in this regime and can be further obscured by slow Larmor precession. Hence, a method of resonant spin amplification is adopted in which the Larmor precision is driven into resonance with the optical excitation repetition interval,  $t_{\text{rep}}$ , by adjusting the applied field. The magnetic field width of the observed resonances is then used to accurately determine the transverse spin lifetime<sup>3</sup>.

Here we apply these methods to the study of mesoscopic lateral spin transport, fabricating samples that permit an externally applied, in-plane voltage. We study undoped and Si-doped ( $1 \times 10^{16} \text{ cm}^{-3}$ ) GaAs substrates, each mechanically polished to a thickness of 30  $\mu\text{m}$  and then uniformly contacted on one face with standard AuGeNi except in a  $\sim 560\text{-}\mu\text{m}$  linear gap where optical studies are performed. A second sample of the Si-doped GaAs is prepared by wet etching to a thickness of  $\sim 2.2 \mu\text{m}$ , as determined by an increase in resistivity. Voltage leads are connected, and the samples are mounted in a magneto-optical cryostat for study in the Voigt configuration, the thicker samples freely suspended and the thinner sample bonded with transparent wax to a fused silica substrate. The gap orientation induces electric fields along the direction of the magnetic field. A miniature Hall sensor records the applied field, and the temperature is regulated at 1.6 K within superfluid  $^4\text{He}$ . A mode-locked Ti:sapphire laser supplies a 1.51-eV pulse train at 76 MHz and 360- $\mu\text{W}$  average power that is split into time-delayed pump and probe beams which overlap as they pass through the sample. The subsequent Faraday rotation of the probe beam is detected by a polarization bridge technique<sup>3</sup>. A stepper motor is used to adjust the lateral pump–probe separation on the

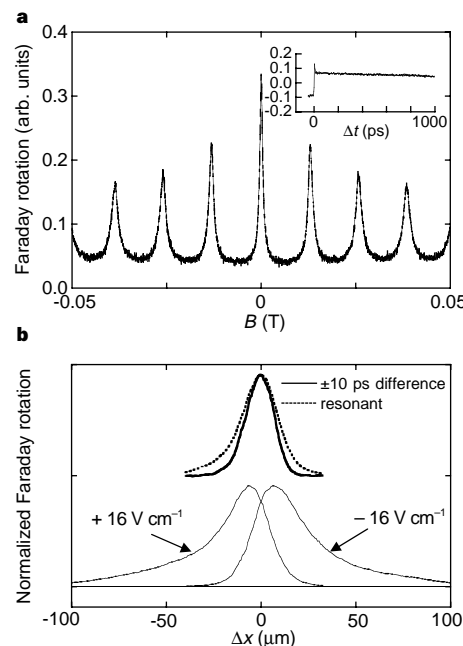


**Figure 1** Pump-probe Faraday rotation measures spin polarization in time, magnetic field and space. **a**, Faraday rotation versus magnetic field for the 30- $\mu\text{m}$ -thick,  $1 \times 10^{16} \text{ cm}^{-3}$  Si-doped GaAs sample. Each peak results from the constructive reinforcement of successive pump pulses. Data are taken with a 100- $\mu\text{m}$  pump diameter and a tightly focused probe. Inset, Faraday rotation versus pump-probe delay taken at a field of 0.0030 T. **b**, Spatial scans of the pump-probe interaction with 12- $\mu\text{m}$  FWHM beams, normalized and offset in amplitude for clarity. The dotted line is the resonant response at  $\Delta t = 0 \text{ ps}$  and  $B = 0$ , and the thick solid line shows the unbroadened spin injection profile, obtained by subtracting the corresponding data at  $\Delta t = -10 \text{ ps}$ . The lower data are taken at  $B = 0$  with applied fields of  $\pm 16 \text{ V cm}^{-1}$ .

sample,  $\Delta x$ , along the direction of the in-plane electric field. In this manner, we are able to study the spatiotemporal profile of the optically excited spin polarization.

Figure 1a shows seven spin resonances near zero field in the Si-doped sample, obtained by scanning the magnetic field ( $B$ ) at  $\Delta t = 50$  ps. The inset shows the associated temporal behaviour of the spin polarization taken slightly off the  $B = 0$  T resonance, with the offset at zero time delay arising from the injection of new spins on the arrival of the pump pulse. We note that pump–probe pairs reappear at 76 MHz, and past spin injections leave an imprint of negative polarization at  $\Delta t < 0$  (ref. 3). The time scans are susceptible to inadvertent changes in beam overlap and focus with delay movement, so we reduce these effects by defocusing the pump. In contrast, spatial scans of the pump–probe overlap are taken at a fixed delay with the pump maximally focused, as shown in Fig. 1b for a field of  $B = 0$  T. No precession occurs at this field, so spin accumulates from consecutive pump pulses, and the spatial profile at any given delay is broadened because of spin diffusion. Nonetheless, the spin injection profile may be extracted by taking the difference signal between scans obtained immediately before and after spin injection ( $\Delta t = \pm 10$  ps). The upper part of Fig. 1b compares the spatial profile obtained by this method (solid line) to the wider profile taken at  $\Delta t = -10$  ps (dotted line). The full-

width at half-maximum (FWHM) of the former ( $18 \mu\text{m}$ ) sets the spatial resolution of our measurements.

The application of an in-plane electric field results in a macroscopic displacement of the electron spin polarization, as shown in lower portion of Fig. 1b for a field of  $\pm 16 \text{ V cm}^{-1}$ . We note that because these data are taken at  $\Delta t = -10$  ps, the last pump pulse has arrived  $\sim 13$  ns before the probe's arrival, so it is possible for there to be a greatly reduced signal at  $\Delta t = 0$ . In addition to the lateral displacement of the spin distribution, its profile becomes asymmetrical. Assuming that the total spin response  $\mathbf{M}$  is the sum of non-interacting spin packets<sup>3</sup>,  $\mathbf{M}(\Delta x, \Delta t) = \sum_n \mathbf{m}_n(\Delta x, \Delta t) = \sum_n \mathbf{m}_n(\Delta x, \Delta t + nt_{\text{rep}})$ , we can understand this asymmetry as arising from a separation of the zero-field spin resonance into its constituents  $\mathbf{m}_n$  created by distinct pump events. In the presence of an electric field, these spins no longer constructively reinforce each other at the resonance magnetic fields because they drift variable distances that are proportional to their ages. Despite an exponential time decay of the spin polarization that leads to a spatial decay along the drift direction, spin transport is observable at distances exceeding  $100 \mu\text{m}$  in rather modest electric fields and mobilities<sup>3</sup>. Our data confirm that (1) the spin polarization measured is that of free electrons with a drift distance linear in electric field, and (2) the spins are carried by negative charges—that

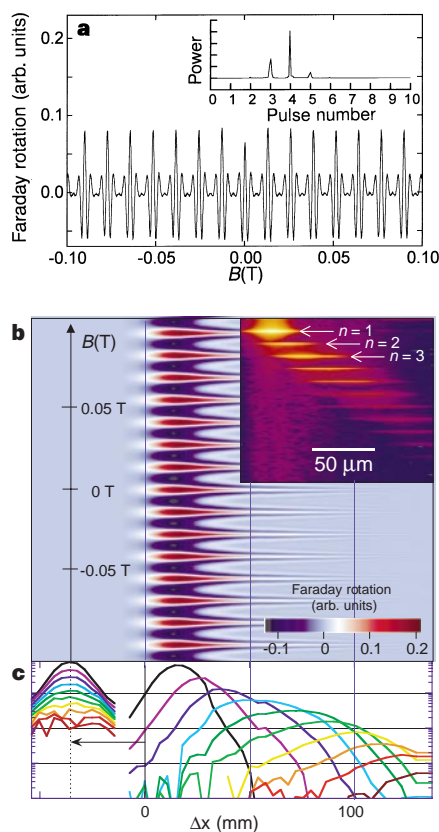


**Figure 2** Macroscopic lateral spin transport as resolved by Fourier decomposition. **a**, Faraday rotation versus magnetic field at a displacement of  $54 \mu\text{m}$  and an electric field of  $-37 \text{ V cm}^{-1}$ . Inset, relative spectral powers of the  $\mathbf{m}_n$  pulses at this location, indexed by  $n$ . **b**, Faraday rotation versus magnetic field and displacement. The field range is the same as in **a** and  $\Delta x$  values are taken from the axis of **c**. Inset, the spectral power of the  $\mathbf{m}_n$  pulses over the range  $-11 \mu\text{m} < \Delta x < 137 \mu\text{m}$ . The first three pulses are labelled by their index,  $n$ . **c**, Amplitudes of the first ten  $\mathbf{m}_n$  constituents versus displacement, obtained by explicit fits to the data in **b** and shown on a logarithmic scale. The  $\mathbf{m}_n$  profiles at zero bias are also shown, displaced  $-36 \mu\text{m}$  for clarity. Sample and excitation remain unchanged from Fig. 1b.

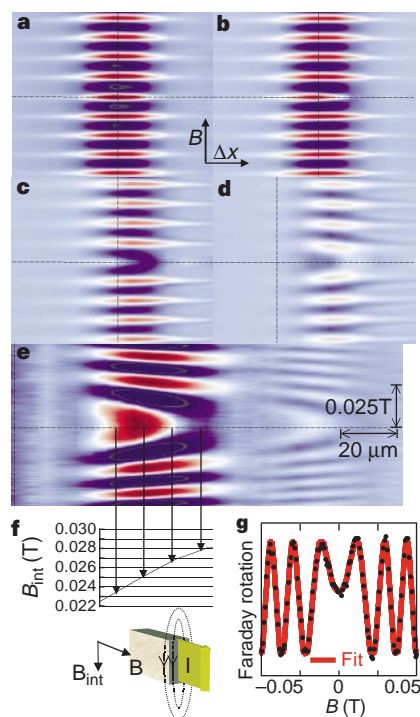


**Figure 3** Self-induced dephasing of spin currents. **a–e**, Faraday rotation in the thinner sample versus magnetic field and displacement for voltages of 0,  $-9.2$ ,  $-18$ ,  $-37$  and  $-92.5 \text{ V cm}^{-1}$ , respectively. The data are taken at  $\Delta t = -10$  ps, so that the youngest spin packet is  $\sim 13$  ns old. The colour scheme is the same as in Fig. 2, except in **e** where the contrast has been enhanced. Vertical and horizontal dashed lines indicate zero displacement and field, respectively, and the scale bars in **e** apply to **a–d** as well. **f**, The internal magnetic field at positions  $32.5 \mu\text{m} < \Delta x < 81.2 \mu\text{m}$  within the most recent spin injection, deduced from a model in which  $B_{\text{int}}$  is generated by currents within the sample (see drawing). The  $\Delta x$  scale is the same as in **e**. **g**, A cross-section of **e** at  $\Delta x = 36 \mu\text{m}$ . Points indicate the measured Faraday rotation versus magnetic field, and the solid red line is a fit to the model described within the text. Excitation remains unchanged from Fig. 1b.

is, we observe electron spins rather than hole spins. The latter has been assumed in a number of spin precession measurements on zinc blende semiconductors<sup>3–5</sup>, and we believe that these data provide direct evidence that Faraday-rotation measurements are truly selective in measuring electron spins. We do not observe any spin polarization travelling oppositely to the electron spins, so the assumption that hole spins scatter rapidly in these systems appears to be valid<sup>5,6</sup>. In the insulating (undoped) control sample, no changes in spin profile are observed at fields up to 400 V cm<sup>-1</sup>.

To obtain a more precise measurement of spin drift in these systems, we note that each constituent of the spin resonance has a different periodicity,  $g\mu_B(\Delta t + nt_{\text{rep}})/\hbar$ , in the applied magnetic field,  $B$ . Thus, by varying  $B$  at each displacement, we can separately identify the spatial extent of the various  $\mathbf{m}_n$  by Fourier decomposition. Figure 2a shows the Faraday rotation versus magnetic field profile taken at a displacement of  $\Delta x = 54 \mu\text{m}$  from the injection point and a pump–probe delay of  $\Delta t = -10$  ps. An applied electric field of  $-37 \text{ V cm}^{-1}$  creates a measurable spin polarization at this lateral position, and harmonic analysis (Fig. 2a inset) reveals that the oscillatory behaviour arises from Larmor precession of the third, fourth and fifth most recent pump pulses. By obtaining field scans over a range in  $\Delta x$ , we may track the spatial position of successive spin packets, as indexed by their injection time. Figure 2b shows a two-dimensional assembly of field scans similar to Fig. 2a, taken from  $\Delta x = -54 \mu\text{m}$  to  $+137 \mu\text{m}$ . A narrowing of the spin resonances and an increasing periodicity in field accompanies lateral displacement, reflecting increased pulse ages with increased  $\Delta x$ . Figure 2b inset shows the corresponding harmonic power versus position, showing that pulse ages increase in steps of  $t_{\text{rep}}$ . The data can thus be used to mark the positions of individual spin packets, and indicate that spin drift is linear in time and corresponds to a drift mobility  $\mu_d = 3 \times 10^3 \text{ cm}^2 \text{ V}^{-1} \text{ s}^{-1}$ .

By explicitly fitting the oscillatory data to obtain the amplitude of each spin packet at every position, we compare the profiles of the ten most recent spin injections at zero and  $-37 \text{ V cm}^{-1}$  in Fig. 2c, where the former are laterally displaced for clarity. These data provide a quantitative measure of spin drift and diffusion over a 130-ns interval following spin injection. To remove artefacts from a strongly field-dependent transverse spin lifetime in the zero-bias sample, these data are obtained by fitting only the  $B = 0$  T spin resonance. As seen on the logarithmic amplitude scale, the zero-bias spins decay exponentially with a characteristic time  $T_2^* = 29$  ns. By fitting the broadening of the spin packet to  $\sqrt{D_s(t + t_0)}$ , where  $t = \Delta t + nt_{\text{rep}}$  is the age of the  $n$ th pulse and  $t_0$  adjusts for its initial width, we obtain a spin diffusion constant  $D_s$  that exceeds the electron diffusion constant,  $D_e = \mu_d kT/e$ , by more than one order of magnitude. This discrepancy suggests that spin diffusion here involves both electron and pure spin diffusion. Applying a voltage does not introduce any severe decoherence ( $T_2^* \sim 17$  ns) and produces a more dramatic profile distortion during transport.

A more subtle effect is a suppression of the  $B = 0$  T spin motion in this sample. Though difficult to distinguish within the colour scale of Fig. 2b, a relative dip in spin polarization appears for  $\Delta x \neq 0$  and fields below a few gauss, as seen in Fig. 2a. Figure 3a–e shows that these effects become stronger in the thinner sample where, as the electric field is increased from 0 to  $-92.5 \text{ V cm}^{-1}$ , the  $B = 0$  T resonance disappears completely and is eventually replaced by neighbouring resonances. These data suggest that electric current flow generates an additional internal magnetic field,  $B_{\text{int}}$ , that dominates near zero external magnetic field. Figure 3g shows a cross-section of the most recent spin packet, separated from other spins by an electric field of  $-92.5 \text{ V cm}^{-1}$ . The data deviate from an expected cosinusoidal behaviour and are more accurately described by an effective field strength,  $B_{\text{eff}}^2 = B_{\text{int}}^2 + B^2$ , with  $B_{\text{int}} = 0.023$  T. A change in the effective magnetic field within the profile of each packet is evident from the shift of the resonances to lower field

strengths at larger displacements. This behaviour cannot be explained by a variation of  $g$ -factors throughout the profile of the spin packet because the Larmor frequency at larger magnetic fields is independent of  $\Delta x$  (not shown). Hence by fitting the field dependence of the Faraday rotation at different  $\Delta x$ , we obtain a profile of the internal magnetic field strength throughout the most recent pulse (Fig. 3f, top). This field distribution leads to inhomogeneous dephasing of the spin direction within each spin packet and scales linearly with the electric field. Similar fits for the thicker sample indicate an internal field that is two orders of magnitude smaller.

Although the magnetic field generated by electric current is of the correct geometry (Fig. 3f, bottom), it changes sign in passing from the front to the back face of the sample whereas the data are well fitted by a single internal field at each  $\Delta x$ . Moreover, for uniform current flow the field strength should scale linearly with the thickness of the sample, while the opposite trend is observed in our data; rough estimates of the surface field strength give the correct order of magnitude for the thicker sample but fail for the thinner sample. One possible explanation is that the optical injection creates a significantly non-uniform, and perhaps filamentary, current flow<sup>7</sup>. Further consideration must also be given to the inherent spin splitting that is known to occur in the conduction band of GaAs away from zero wavevector<sup>8</sup>. We find it difficult to identify  $B_{\text{int}}$  solely with the corresponding effective field, however, as the latter is linearly proportional to and uniquely determined by the drift velocity<sup>8</sup> whereas the former is dramatically different in thick and thin samples with the same drift velocity. □

Received 4 August; accepted 5 November 1998.

1. Prinz, G. Spin-polarized transport. *Phys. Today* **48**, 58–63 (1995).
2. Kane, B. E. A silicon based nuclear spin quantum computer. *Nature* **393**, 133–137 (1998).
3. Kikkawa, J. M. & Awschalom, D. D. Resonant spin amplification in GaAs. *Phys. Rev. Lett.* **80**, 4313–4316 (1998).
4. Kikkawa, J. M., Smorchkova, I. P., Samarth, N. & Awschalom, D. D. Room-temperature spin memory in two-dimensional electron gases. *Science* **277**, 1284–1287 (1997).
5. Worsley, R. E., Traynor, N. J., Grevatt, T. & Harley, R. T. Transient linear birefringence in GaAs quantum wells. *Phys. Rev. Lett.* **76**, 3224–3227 (1996).
6. Oestreich, M. *et al.* Temperature and density dependence of the electron Landé  $g$ -factor in semiconductors. *Phys. Rev. B* **53**, 7911–7916 (1996).
7. Niedernostheide, F.-J., Hirsinger, J., Prettl, W., Novak, V. & Kostial, H. Oscillations of current filaments in n-GaAs caused by a magnetic field. *Phys. Rev. B* **58**, 4454–4458 (1998).
8. Kalevich, V. K. & Korenov, V. L. Effect of electric field on the optical orientation of 2D electrons. *Pis'ma Zh. Eksp. Teor. Fiz.* **52**, 230–235 (1990) [*JETP Lett.* **52**, 230–235 (1990)].

**Acknowledgements.** We thank S. J. Allen for discussions and acknowledge support from the ARO and NSF QUEST STC.

Correspondence and requests for materials should be addressed to D.D.A. (e-mail: awsch@physics.ucsb.edu).

## Entropic trapping of macromolecules by mesoscopic periodic voids in a polymer hydrogel

Lei Liu\*†, Pusheng Li\*† & Sanford A. Asher\*

\* Department of Chemistry, University of Pittsburgh, Pittsburgh, Pennsylvania 15260, USA

**The separation of macromolecules such as polymers and DNA by means of electrophoresis, gel permeation chromatography or filtration exploits size-dependent differences in the time it takes for the molecules to migrate through a random porous network. Transport through the gel matrices, which usually consist of full swollen crosslinked polymers<sup>1–11</sup>, depends on the relative size of**

† Present address: Praxair Service Technologies Inc., 1555 Main St, Indianapolis, Indiana 46254, USA (L.L.); Epsilon Inc., HPOS, 50 Cambridge St, Burlington, Massachusetts 01803, USA (P.L.).